
DC-Gaussian: Improving 3D Gaussian Splatting for Reflective Dash Cam Videos

Linhan Wang¹ Kai Cheng³ Shuo Lei⁶ Shengkun Wang¹ Wei Yin⁴

Chenyang Lei⁵ Xiaoxiao Long^{2†} Chang-Tien Lu¹

¹Virginia Tech ²Hong Kong University ³USTC ⁴University of Adelaide ⁵CAIR ⁶Sony Research



Figure 1: Given a sequence of video captured by a dash cam that may contain obstructions like reflections and occlusions, **DC-Gaussian** achieves high-fidelity novel view synthesis getting rid of the obstructions. (a) dash cam; (b) original video frame; (c) novel view rendering with obstruction removal.

Abstract

We present DC-Gaussian, a new method for generating novel views from in-vehicle dash cam videos. While neural rendering techniques have made significant strides in driving scenarios, existing methods are primarily designed for videos collected by autonomous vehicles. However, these videos are limited in both quantity and diversity compared to dash cam videos, which are more widely used across various types of vehicles and capture a broader range of scenarios. Dash cam videos often suffer from severe obstructions such as reflections and occlusions on the windshields, which significantly impede the application of neural rendering techniques. To address this challenge, we develop DC-Gaussian based on the recent real-time neural rendering technique 3D Gaussian Splatting (3DGS). Our approach includes an adaptive image decomposition module to model reflections and occlusions in a unified manner. Additionally, we introduce illumination-aware obstruction modeling to manage reflections and occlusions under varying lighting conditions. Lastly, we employ a geometry-guided Gaussian enhancement strategy to improve rendering details by incorporating additional geometry priors. Experiments on self-captured and public dash cam videos show that our method not only achieves state-of-the-art performance in novel view synthesis, but also accurately reconstructing captured scenes getting rid of obstructions. project page

1 Introduction

Neural Radiance Field (NeRF) [29] has revolutionized the image-based rendering area with its differentiable volume rendering technique. 3D Gaussian Splatting (3DGS) [19] pushes the frontier further with real-time rendering speed. These technologies have been applied to datasets captured by autonomous cars [41, 6, 25], opening up numerous new possibilities in autonomous driving, such as simulating driving scenarios [55, 50] for robust training of perception models and providing effective 3D scene representations to enhance comprehensive environmental understanding [14, 61, 64]. Although these datasets provide multi-modality sensor data, their diversity in real-world driving scenarios is still limited [7].

Fortunately, dash cam videos deeply reflect the diversity and complexity of real-world traffic scenarios [8]. They are used to provide large-scale, diverse driving video datasets in a crowd-sourced manner [57]. Dash cam videos also offer unique value by capturing multi-agent driving behaviors [7] and evaluating the robustness of algorithms under visual hazards [58]. Moreover, the global dash cam market is rapidly expanding, driven by increasing awareness of vehicular safety [33]. Therefore, the exploration of utilizing dash camera data in neural rendering shows great potential, offering enormous amounts of data for autonomous driving applications.

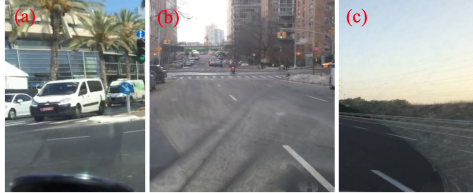


Figure 2: Common obstructions on windshields: (a) Mobile-phone holder; (b) Reflections; (c) Stains.

However, naively training 3DGS on dash cam videos often results in a significant deterioration of rendering quality and geometry. This degradation is primarily due to the common existence of obstructions (reflections and occlusions such as mobile phone holders and stains, as shown in Fig. 2) on windshields. In these scenarios, 3DGS models the obstructions as stationary geometries while they are dynamic in nature (moving with cars), thus unavoidably causing inaccurate geometry and blurry renderings in novel views.

Although some single-image-based obstruction removal methods exist, directly applying them to this task is nontrivial. These obstructions arise from various sources, while existing removal methods impose strict assumptions on obstructions [12, 62, 54, 53, 37, 20]. For instance, assumptions like out-of-focus [62] and ghost cue [37] allow previous methods to perform well in specific cases, but these assumptions don't always hold in dash cam videos. Moreover, the performance of learning-based methods degrades for out-of-distribution images [46, 27, 21]. Several NeRF methods [16, 32, 66, 67] attempt to reconstruct scenes with reflections by decomposing transmission (background scene) and reflection with independent NeRFs. This approach can benefit from the strong multi-view aggregation power of NeRF. However, previous methods are insufficient for dash cam videos because the obstructions on windshields do not align well with NeRF's design. The vanilla NeRF is intended for static scenes, whereas windshields and their reflected objects move with the cars.

In this paper, we introduce DC-Gaussian, a method for modeling high-fidelity obstruction-free 3D Gaussian Splatting from dash cam videos. We introduce three key innovations: 1) **Adaptive image decomposition**. To clearly decompose images with complex reflections and occlusions, we propose an adaptive image decomposition approach. We use an opacity map to learn the transmittance of the windshield, which adaptively estimates the contribution of the background scene to the image. 2) **Illumination-aware Obstruction Modeling (IOM)**. We observe that the obstructions are mainly caused by the objects being relatively static with the dash camera, but the obstructions present varying effects due to changing illumination. We therefore propose modeling global obstructions that are shared for all views. Moreover, a novel **Latent Intensity Modulation (LIM)** module is introduced to learn the illumination changes from the scene and enable synthesis of reflection with varying intensity. 3) **Geometry-guided Gaussian Enhancement (G3E)**. We further leverage multi-view stereo to introduce geometry prior into 3DGS training, which enhances the details and sharpness of 3DGS rendering.

To evaluate the efficacy of our method, we conduct extensive experiments on public datasets [57] and a self-captured dataset. The experiments show that our method not only achieves state-of-the-art novel view synthesis, but also clearly removes obstructions from neural rendering.

2 Related work

2.1 Novel view synthesis for driving scenes

Novel view synthesis aims to render novel views given posed images of the same scene. NeRF [29], which combines multiple layer perceptions and differentiable volume rendering, initiated a revolution in this area by rendering photorealistic images. Subsequent works [3] [59] extended NeRF to unbounded large-scale scenes by warping the space into a bounded cube. BlockNeRF [43] first introduced NeRF to driving scenes by dividing the scenes into blocks and training separate models on them. The method of scene division was further improved in later works [44, 63]. To apply NeRF to multi-camera systems, UC-NeRF [10] addresses the under-calibration problem by refining the poses with spatio-temporal constraints. S-NeRF [51] uses sparse LiDAR points to enhance the training of NeRF and learn robust geometry. Decomposing dynamic objects and static backgrounds in driving scenes presents another challenge. Some works [45, 52] tackle this challenge with the help of LiDAR and 2D optical flows.

Recently 3DGS [19] has attracted great attention in the research community. It achieves optimal results in novel view synthesis and rendering speed by explicitly modeling a 3D scene with 3D Gaussians. Some researchers have extended it to dynamic objects and scenes. Given a set of dynamic monocular images, a deformation network is introduced to model the motion of Gaussians [56]. DrivingGaussian [65] models and decomposes dynamic driving scenes based on composite Gaussian splatting. GaussianPro [9] improves the geometry of 3DGS by controlling the densification process of 3DGS with classic PatchMatching algorithm [2]. Zhou et al. [64] proposed to utilize 3D Gaussian Splatting for holistic urban scene understanding. However, dash cam videos, an important data source for understanding driving scenes, remain unexplored due to obstructions on the windshield. Despite previous works [65, 52, 56] making progress in separating dynamic objects from background scenes, the image decomposition problem we are addressing presents unique challenges because of the obstructions' transparent or semi-transparent nature.

2.2 Obstruction removal and layer separation

Single-image reflection removal. To address the highly ill-posed problem of single-image reflection removal, various methods leverage different cues. Polarization cues are particularly valuable as they are inherently present in all natural light sources [35, 13, 21, 28]. Gradient priors [23, 24, 1] are utilized based on the observation that reflection and background layers often exhibit different levels of sharpness. Additionally, ghosting cues [37, 62, 18] and flash/non-flash pairs [20, 22] can be effective in certain scenarios. However, these assumptions do not always hold in real-world situations. With the advancement of deep learning technology, learning-based methods [17, 12, 49, 17] have been developed to model reflection properties more comprehensively. Despite their success, reflection removal from a single image remains challenging due to the inherently ill-posed nature of the problem, the absence of motion cues [27], and the difficulties in out-of-domain generalization [46].

Multi-image layer separation. Existing methods often exploit differences in motion patterns between transmission and obstruction layers and use learned image priors [15] to decompose images into multiple components. These layer separation methods estimate dense motion fields for each layer using optical flow [42], SIFT flow [39], and deep learning-based flow estimation methods [40, 27]. Recently, Nam et al. [31] proposed a multi-frame fusion framework based on neural image representation, achieving strong performance on various layer-separation tasks. Similarly, NSF [11] fuses RAW burst image sequences by modeling optical flow with neural spline fields. However, methods designed for burst images struggle with large pixel motions in driving scenes.

NeRF with reflections. NeRFren [16] is the pioneering work that adapts NeRF to model scenes with reflections by proposing to model transmitted and reflected components with separate NeRFs. NeuS-HSR [32] achieves high-fidelity 3D surface reconstruction by explicitly modeling the glasses with an auxiliary plane module. Zhu et al. [66] introduce recurring edge cues to achieve robust results under sparse views. However, previous methods are insufficient for dash cam videos because the obstructions on windshields do not align well with NeRF's design. The vanilla NeRF is intended for static scenes, whereas windshields and their reflected objects move with the cars. The varying illumination in the wild makes reflections modeling even more challenging. In contrast to existing methods, our proposed obstruction modeling approach leverages the static nature of obstructions in camera coordinates and captures the varying intensity of reflections.

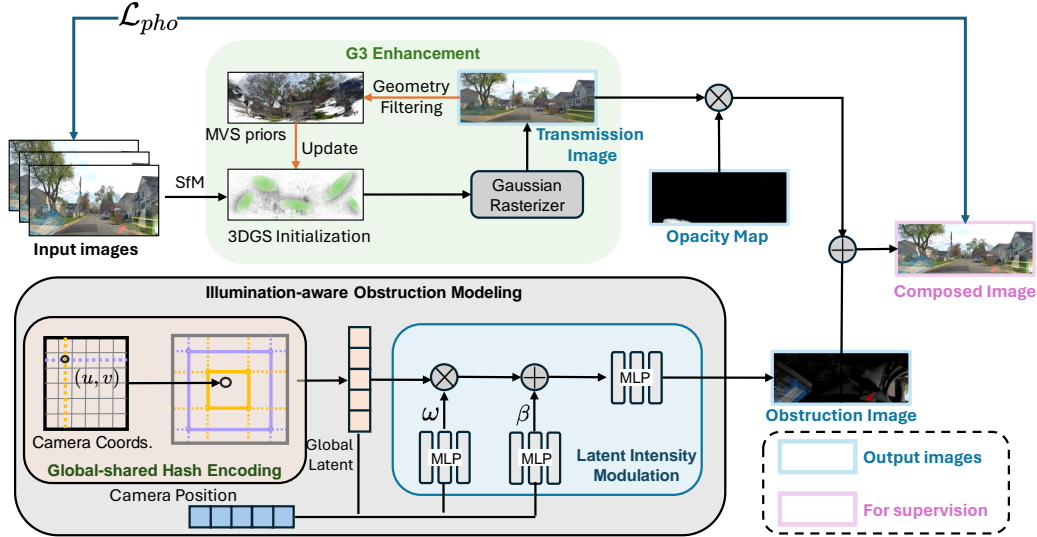


Figure 3: Overview of DC-Gaussian framework. To model obstructions with different opacities in a unified manner, we use an learnable opacity map to adaptively reweight the contribution of transmission. The global-shared multiresolution hash encoding is introduced to fully utilize the static motion prior of obstructions. We propose a Latent Intensity Modulation module to grasp the intensity changes of reflections conditioned on camera positions. Finally, in the G3 Enhancement module, we run geometry filtering on obstruction-suppressed images to enhance the geometry of 3D Gaussians.

3 Method

Our DC-Gaussian extends the standard 3DGS to corrupted dash cam videos. We begin by reviewing the standard 3DGS pipeline 3.1. Then we introduce the adaptive image decomposition 3.3 to decompose the reflections and occlusions from the corrupted dash cam images. In 3.3, we propose the Illuminate-aware Obstruction Modeling module. A novel Latent Intensity Modulation is introduced to enable high quality modeling of reflection even under vary illumination. Finally, the geometry guided Gaussian enhancement strategy is explained in 3.4.

3.1 Preliminary of 3D Gaussian Splatting

3DGS [19] models the 3D scene as a set of 3D Gaussians. Each 3D Gaussian G is defined as:

$$G(\mathbf{x}) = e^{-\frac{1}{2}(\mathbf{x}-\boldsymbol{\mu})^T \boldsymbol{\Sigma}^{-1}(\mathbf{x}-\boldsymbol{\mu})} \quad (1)$$

where $\boldsymbol{\mu}$ and $\boldsymbol{\Sigma}$ represent its mean vector and covariance matrix, respectively. For optimization purpose, the covariance matrix is further expressed as $\boldsymbol{\Sigma} = \mathbf{R}\mathbf{T}\mathbf{S}^T\mathbf{R}^T$, where \mathbf{S} and \mathbf{R} are the scaling matrix and rotation matrix, respectively. To render an image, the splatting technique [68] is applied. Specifically, the color of each pixel \mathbf{p} is calculated by blending N ordered Gaussians $\{G_i | i = 1, \dots, N\}$ overlapping \mathbf{p} as:

$$\mathbf{c}(\mathbf{p}) = \sum_{i=1}^N \mathbf{c}_i \alpha_i \prod_{j=1}^{i-1} (1 - \alpha_j) \quad (2)$$

where α_i is obtained by evaluating a projected 2D Gaussian [68] from G_i at \mathbf{p} multiplied with a learned opacity of G_i , and \mathbf{c}_i is the learnable color of G_i .

3.2 Adaptive image decomposition

To synthesize images with obstructions, previous methods [16, 32] render **transmission image** I_t and **obstruction image** I_o separately and utilize a naive linear combination of I_t and I_o to render the final output I , as illustrated in Eq. 3:

$$I = \phi_1 * I_t + \phi_2 * I_o, \quad (3)$$

where ϕ_1 and ϕ_2 are manually chosen. While this approach achieves descent performance on the pure reflection corrupted images, it cannot achieve good performance on dash cam videos with complex obstructions. Among the common obstructions, mobile-phone holders are opaque, stains is semi-transparent and reflections are transparent. Faced with this complex situation, inspired by [31], we propose to learn the opacity map ϕ from the input images. As a result, we reformulate the rendering process:

$$I(u, v, j) = (1 - \phi)I_t(u, v, j) + I_o(u, v, j) \quad (4)$$

where $u, v \in [0, 1]$ are the continuous image coordinates and $j \in [0, 1, \dots, N - 1]$ is the frame number. Instead of defining the opacity field in 3D world space, we define the opacity relative to the 2D image space of each view. This approach is more convenient for modeling obstructions because view-dependent effects are only related to the training images. In this image decomposition method, the transmission images represent the driving scenes viewed through the windshield. We can use standard 3DGS to model these scenes due to its multi-view consistent property. Thus, $I_t(u, v, j)$ can be easily calculated by Eq. 2, given the camera pose of frame j . I_o represents the appearance of the complex obstructions on the windshield. We explain its modeling in the next section.

3.3 Illumination-aware Obstruction Modeling

Decomposing the images into transmission and obstruction is challenging due to the strong ambiguity between the two components. It is an ill-posed problem without prior information. We have two observations about the obstructions on the windshield that can strongly mitigate this ambiguity.

Observation 1 As shown in Fig. 4 (a), the reflections on the windshields are from objects (air conditioner vent) inside the car, which means they are relatively stationary with the car [38]. Additionally, occlusions are attached to the windshields, which are also relatively stationary with the car. Consequently, we can assume that the appearance of the obstructions is like an image shared globally by all the frames in a dash cam video.

Observation 2 As cars move along the road, the trees and buildings on the sides occasionally block the incident light, affecting the intensity of the reflections. For example, under strong light, reflections are also strong, as shown in Fig. 4 (a), while the reflections "disappear" under weak light, as seen in Fig. 4 (d). Thus, the strength of the reflections is conditioned on the car's position.

These two observations require us to design a model for obstructions that takes advantage of the global-sharing property of obstructions and also grasps varying intensity reflections conditioned on the car's position.

Global-shared Multi-resolution Hash Encoding. To align our design with Observation 1, we use a global-shared latent representation for obstructions' appearance. Specifically, we use continuous image coordinates $u, v \in [0, 1]$ as the input. Then we use a multi-resolution hash encoder γ [30] to map these coordinates into high-dimensional learnable latent features. For example, we use an L level hash encoder where each level stores F dimensional features. Thus, each u, v pair maps to an $L * F$ dimensional latent features $\gamma(u, v)$. While our method is not restricted to this specific type of spatial encoding, we choose the multi-resolution hash encoder for two reasons. First, its hierarchical multi-resolution representation can adaptively learn the obstruction appearance in a coarse-to-fine fashion. Second, its efficient implementation matches the speed of 3DGS, without slowing down the training significantly.

Latent Intensity Modulation. In order to accurately capture the intensity variations in environmental lighting conditioned on car positions, we propose a novel Latent Intensity Modulation (LIM) module. Specifically, to enable selective activation of reflections conditioned on camera positions, we design a



Figure 4: When the intensity of incident light changes, the strength of reflections also change accordingly (a)(d). Our method achieves high-fidelity reflections synthesis (c)(f) and reasonable decomposition results (b)(e) under varying light. The reflections in (f) are brightened to reveal details.

Scaling Gate ω and an *Offset Gate* β , which are generated by two MLPs with the concatenation of camera positions π_j and $\gamma(u, v)$ as input.

$$\omega(u, v, \pi_j) = \text{MLP}([\pi_j, \gamma(u, v)]), \beta(u, v, \pi_j) = \text{MLP}([\pi_j, \gamma(u, v)]), \quad (5)$$

Then, the latent features are modulated element-wise through these two gates. Finally, we use a MLP to decode the modulated latent features into RGB information of obstructions.

$$I_o(u, v, \pi_j) = \text{MLP}(\omega(u, v, \pi_j) \odot \gamma(u, v) + \beta(u, v, \pi_j)) \quad (6)$$

With the LIM module, our method achieves effective image decomposition and synthesizes high-fidelity reflections under varying light conditions, as shown in Fig. 4.

3.4 Geometry-guided Gaussian Enhancement

In IOM, we utilize the motion pattern prior of obstructions to reduce ambiguity in decomposing images. Despite this, some ambiguity still remains. To further enhance performance, we incorporate geometry priors. Typically, strong obstructions affect only portions of the images. As cars move, the same areas in the 3D world can appear in several image fragments which are not or less interfered with by obstructions. In these image fragments, capturing the same areas from different angles, ambiguity is minimal due to the dominance of transmission. Based on this intuition, we leverage a multi-view stereo (MVS) algorithm to identify these "image fragments" and generate geometry priors for 3D Gaussians.

Specifically, we employ a deep MVS method [47] to generate depth maps for all views. A geometric consistency filtering process [36] is leveraged to generate masks M_j masking the multi-view consistent areas, which are essentially the "image fragments" we want to identify. The masked depth maps are then mapped to 3D space as dense point clouds, which are used to initialize 3D Gaussians at physically accurate positions. To find more multi-view consistent "image fragments," we propose suppressing the obstructions in training images by employing our proposed method. Specifically, we remove obstructions from input images to obtain transmission \hat{I}_t^j . For areas blocked by occlusions, we inpaint the content with I_t^j .

$$\hat{I}_t^j = \begin{cases} (I^j - I_o^j)/(1 - \phi), & \text{if } \phi < \tau \\ I_t^j & \text{otherwise} \end{cases} \quad (7)$$

Here I^j is the j_{th} input image. I_o^j and I_t^j are synthesized by trained IOM and 3DGS, respectively. We use 0.5 for the threshold τ in all the experiments.

3.5 Implementation details

We develop our method based on 3DGS. We borrow multi-resolution hash encoding and fast MLP implementation from tiny-cuda-nn [30] to build IOM. We choose PatchMatchNet [47] as the MVS

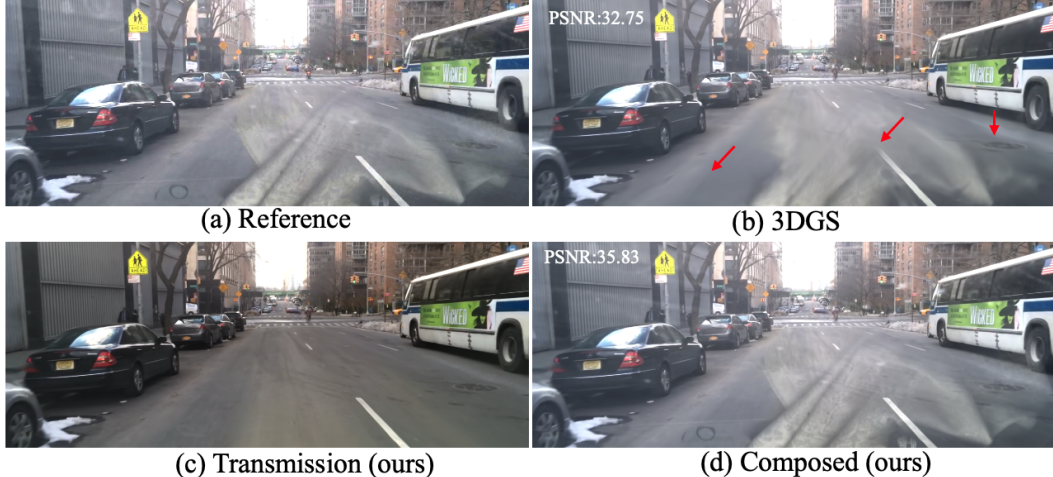


Figure 5: Comparisons with 3DGS on novel view synthesis. Because the obstructions violate multi-view consistency, the performance of 3DGS degrades significantly, resulting in artifacts and blurry renderings (highlighted by red arrows). In contrast, our method not only faithfully synthesizes novel view renderings but also renders transmission with fine details.

method in G3E. We follow previous driving scenes reconstruction works [45, 10] to separately model the sky areas. We use a L_1 loss $\mathcal{L}_{opacity}$ to regularize the opacity field. The final loss function is:

$$\mathcal{L} = \mathcal{L}_{pho} + \lambda_1 \mathcal{L}_{sky} + \lambda_2 \mathcal{L}_{opacity} \quad (8)$$

\mathcal{L}_{pho} is the same as in standard 3DGS [19]. \mathcal{L}_{sky} is borrowed from UCNeRF [10]. We use 0.001 for both λ_1 and λ_2 . We run all the experiments with an A100 GPU. Each scene contains approximately 300 images in our evaluation datasets. Combined training of the 3DGS and IOM for 30k iterations with Adam optimizer takes about 30 minutes. It takes 40 minutes in total to evaluate MVS and run geometry filtering.

4 Experiments

4.1 Datasets

BDD100K. To evaluate the performance of our method and baselines, we adopt BDD100K [57] for evaluation. These scenes are from dash cam videos captured in daily life. They contain common obstructions, such as reflections, mobile phone holders, stickers and stains. Evaluation on this dataset reflects performance on real life dash cam videos.

DCVR. To further evaluate the performance of our method on strong reflection conditions, we established **DCVR** (Dash Cam Videos with Reflection) dataset. The original videos are undistorted [5] to ease the structure-from-motion algorithm. We utilize the popular tools COLMAP [36] and HLoc [34, 26] to estimate the camera parameters.

4.2 Baselines

We choose 3DGS as our baseline [19]. We also compare our method with other state-of-the-art method Zip-NeRF [4] and GaussianPro [9]. To evaluate the performance of novel view synthesis, following common settings [3], we select one of every eight images as testing images and the remaining ones for training. Since our method is also designed for image decomposition, we also compare our method with state-of-the-art obstruction removal methods, including DSRNet [17], NIR [31] and Liu et al. [27].

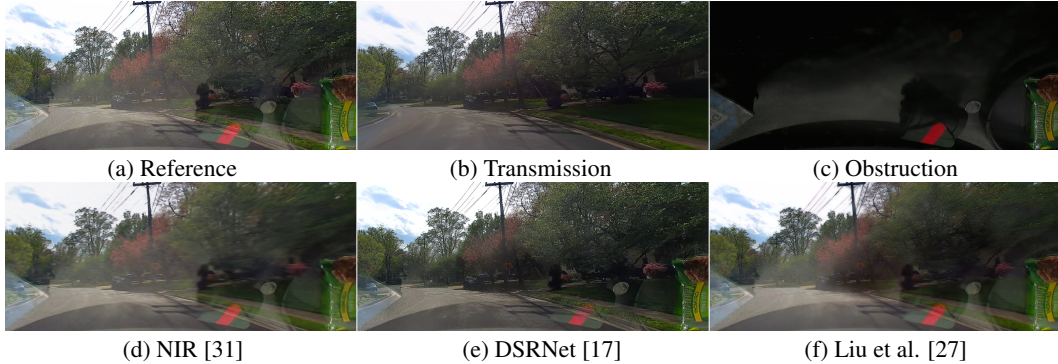


Figure 6: Comparisons with the image-based reflection removal methods on removing reflections. (a) Reference is a frame in a dash cam video. (d), (e), and (f) are results from previous obstruction removal methods, which are not effective in this scenario. In comparison, our method decomposes the image and synthesizes (b) transmission and (c) obstruction with high fidelity.

Table 1: Evaluation of novel view synthesis on BDD100K and DCVR. We indicate the best and second best with bold and underlined respectively. Our method consistently outperforms state-of-the-art methods in both datasets and all the evaluation metrics.

Method	BDD100K			DCVR		
	PSNR \uparrow	SSIM \uparrow	LPIPS \downarrow	PSNR \uparrow	SSIM \uparrow	LPIPS \downarrow
ZipNeRF [4]	27.89	0.875	0.176	24.41	0.786	0.228
GaussianPro [9]	27.75	0.894	0.192	23.71	0.770	0.270
3DGS [19]	<u>28.02</u>	<u>0.897</u>	<u>0.188</u>	23.73	0.783	0.248
DCGaussian (Ours)	29.44	0.914	0.143	24.74	0.822	0.202

4.3 Quantitative results

For the quantitative evaluation, we conduct comparison with baselines on both BDD100K and DCVR. We apply the three widely-used metrics for evaluation, i.e., PSNR, SSIM [48], and LPIPS [60]. The results are shown in Tab. 1. The consistent superior performance of our method shows the efficacy of the proposed modules. Though GaussianPro applies a progressive propagation strategy to enhance the geometry of 3D Gaussians, without separate obstruction modeling, it cannot handle the obstructions corrupted dash cam videos.

4.4 Qualitative results

Novel view synthesis. We show the novel view synthesis results in Fig. 5. Without a proper representation for obstructions, 3DGS can hardly synthesize high-quality obstructions. Moreover, its wrong geometry also results in blurry renderings and artifacts on the road surface. In contrast, our method effectively tackles the ambiguity between obstructions and transmissions and synthesizes both components with high-fidelity. We provide depth map in the appendix.

Table 2: Ablations studies on DCVR. Metrics are calculated on obstruction influenced areas.

NOM	AD	LIM	G3E	PSNR \uparrow	SSIM \uparrow	LPIPS \downarrow
✗	✗	✗	✗	23.99	0.738	0.287
✓	✗	✗	✗	25.21	0.776	0.252
✓	✓	✗	✗	25.65	0.791	0.236
✓	✓	✓	✗	25.90	0.798	0.229
✓	✓	✓	✓	26.30	0.814	0.210

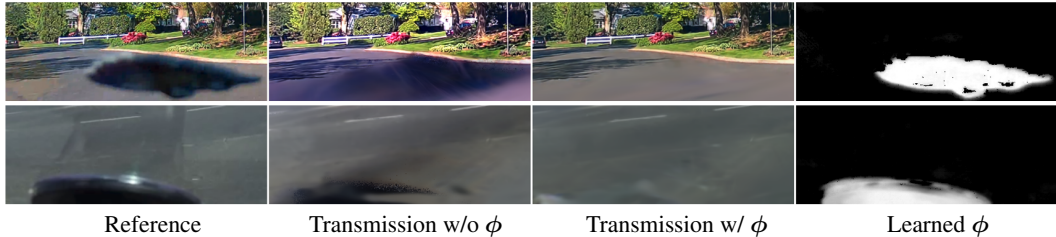


Figure 7: Ablation study about the Learnable opacity map ϕ . The incorporation of the opacity map leads to better view synthesis and obstruction removal.



Figure 8: Ablation study on G3E module. G3E helps suppress artifacts and reveal sharper details.

Obstruction removal. We show the obstruction removal results in Fig. 6. The single image reflection removal method (e) only marginally suppresses reflections. Multi-image layer separation methods (d)(f) struggle with accurate optical flow estimation, resulting in blurry outputs. In comparison, our method models reflections (c) with high quality and retains fine details in transmission (b). These visual results demonstrate our method’s potential in reconstructing obstruction-free driving scenes from dash cam videos.

4.5 Ablation study

We conduct extensive ablation studies on DCVR to explore the impact of each module in DC-Gaussian. Quantitative results are shown in Table 2. To assess the efficacy of global-shared hash encoding, we evaluate 3DGS with a Naive Obstruction Module (NOM), where latent features are directly decoded by an MLP to generate RGB. NOM shows significant improvement over the baseline, demonstrating that global-shared hash encoding effectively leverages the static prior of obstructions in dash cam videos. The adaptive image decomposition (AD) strategy further enhances results by effectively modeling occlusions, as shown in Fig. 7. Additionally, LIM improves performance by capturing intensity changes in reflections. Finally, incorporating geometry priors into 3D Gaussians with G3E effectively suppresses artifacts on the road and reveals sharper details, as illustrated in Fig. 8.

5 Conclusions

In conclusion, we propose DC-Gaussian that effectively addresses the challenges of extending 3D Gaussian Splatting to dash cam videos. Experiments on BDD100K and DCVR demonstrate a significant improvement in rendering quality and images decomposition, setting a new benchmark for neural rendering with dash cam videos.

Limitations and future work Currently, DC-Gaussian has only been evaluated on single-sequence videos. However, considering the vast amount of dash cam footage available, extending DC-Gaussian to a multi-sequence video setting and leveraging dense view images to achieve more pleasing results would be a promising direction for future research.

References

- [1] Nikolaos Arvanitopoulos, Radhakrishna Achanta, and Sabine Susstrunk. Single image reflection suppression. In *Proceedings of the IEEE conference on computer vision and pattern recognition*, pages 4498–4506, 2017.
- [2] Connelly Barnes, Eli Shechtman, Adam Finkelstein, and Dan B Goldman. Patchmatch: A randomized correspondence algorithm for structural image editing. *ACM Trans. Graph.*, 28(3):24, 2009.
- [3] Jonathan T Barron, Ben Mildenhall, Matthew Tancik, Peter Hedman, Ricardo Martin-Brualla, and Pratul P Srinivasan. Mip-nerf: A multiscale representation for anti-aliasing neural radiance fields. In *Proceedings of the IEEE/CVF International Conference on Computer Vision*, pages 5855–5864, 2021.
- [4] Jonathan T Barron, Ben Mildenhall, Dor Verbin, Pratul P Srinivasan, and Peter Hedman. Zip-nerf: Anti-aliased grid-based neural radiance fields. In *Proceedings of the IEEE/CVF International Conference on Computer Vision*, pages 19697–19705, 2023.
- [5] G. Bradski. The OpenCV Library. *Dr. Dobb's Journal of Software Tools*, 2000.
- [6] Holger Caesar, Varun Bankiti, Alex H Lang, Sourabh Vora, Venice Erin Liong, Qiang Xu, Anush Krishnan, Yu Pan, Giancarlo Baldan, and Oscar Beijbom. nuscenes: A multimodal dataset for autonomous driving. In *Proceedings of the IEEE/CVF conference on computer vision and pattern recognition*, pages 11621–11631, 2020.
- [7] Rohan Chandra, Xijun Wang, Mridul Mahajan, Rahul Kala, Rishitha Palugulla, Chandrababu Naidu, Alok Jain, and Dinesh Manocha. Meteor: A dense, heterogeneous, and unstructured traffic dataset with rare behaviors. In *2023 IEEE International Conference on Robotics and Automation (ICRA)*, pages 9169–9175. IEEE, 2023.
- [8] Zhengping Che, Guangyu Li, Tracy Li, Bo Jiang, Xuefeng Shi, Xinsheng Zhang, Ying Lu, Guobin Wu, Yan Liu, and Jieping Ye. D²-city: a large-scale dashcam video dataset of diverse traffic scenarios. *arXiv preprint arXiv:1904.01975*, 2019.
- [9] Kai Cheng, Xiaoxiao Long, Kaizhi Yang, Yao Yao, Wei Yin, Yuexin Ma, Wenping Wang, and Xuejin Chen. Gaussianpro: 3d gaussian splatting with progressive propagation. *arXiv preprint arXiv:2402.14650*, 2024.
- [10] Kai Cheng, Xiaoxiao Long, Wei Yin, Jin Wang, Zhiqiang Wu, Yuexin Ma, Kaixuan Wang, Xiaozhi Chen, and Xuejin Chen. Uc-nerf: Neural radiance field for under-calibrated multi-view cameras. In *The Twelfth International Conference on Learning Representations*, 2023.
- [11] Ilya Chugunov, David Shustin, Ruyu Yan, Chenyang Lei, and Felix Heide. Neural spline fields for burst image fusion and layer separation. *arXiv preprint arXiv:2312.14235*, 2023.
- [12] Qingnan Fan, Jiaolong Yang, Gang Hua, Baoquan Chen, and David Wipf. A generic deep architecture for single image reflection removal and image smoothing. In *Proceedings of the IEEE International Conference on Computer Vision*, pages 3238–3247, 2017.
- [13] Hany Farid and Edward H Adelson. Separating reflections and lighting using independent components analysis. In *Proceedings. 1999 IEEE Computer Society Conference on Computer Vision and Pattern Recognition (Cat. No PR00149)*, volume 1, pages 262–267. IEEE, 1999.
- [14] Xiao Fu, Shangzhan Zhang, Tianrun Chen, Yichong Lu, Lanyun Zhu, Xiaowei Zhou, Andreas Geiger, and Yiyi Liao. Panoptic nerf: 3d-to-2d label transfer for panoptic urban scene segmentation. In *2022 International Conference on 3D Vision (3DV)*, pages 1–11. IEEE, 2022.
- [15] Yosef Gandelsman, Assaf Shocher, and Michal Irani. "double-dip": unsupervised image decomposition via coupled deep-image-priors. In *Proceedings of the IEEE/CVF conference on computer vision and pattern recognition*, pages 11026–11035, 2019.
- [16] Yuan-Chen Guo, Di Kang, Linchao Bao, Yu He, and Song-Hai Zhang. Nerfren: Neural radiance fields with reflections. In *Proceedings of the IEEE/CVF Conference on Computer Vision and Pattern Recognition*, pages 18409–18418, 2022.

- [17] Qiming Hu and Xiaojie Guo. Single image reflection separation via component synergy. In *Proceedings of the IEEE/CVF International Conference on Computer Vision*, pages 13138–13147, 2023.
- [18] Yan Huang, Yuhui Quan, Yong Xu, Ruotao Xu, and Hui Ji. Removing reflection from a single image with ghosting effect. *IEEE Transactions on Computational Imaging*, 6:34–45, 2019.
- [19] Bernhard Kerbl, Georgios Kopanas, Thomas Leimkühler, and George Drettakis. 3d gaussian splatting for real-time radiance field rendering. *ACM Transactions on Graphics*, 42(4):1–14, 2023.
- [20] Chenyang Lei and Qifeng Chen. Robust reflection removal with reflection-free flash-only cues. In *Proceedings of the IEEE/CVF Conference on Computer Vision and Pattern Recognition*, pages 14811–14820, 2021.
- [21] Chenyang Lei, Xuhua Huang, Mengdi Zhang, Qiong Yan, Wenxiu Sun, and Qifeng Chen. Polarized reflection removal with perfect alignment in the wild. In *Proceedings of the IEEE/CVF conference on computer vision and pattern recognition*, pages 1750–1758, 2020.
- [22] Chenyang Lei, Xudong Jiang, and Qifeng Chen. Robust reflection removal with flash-only cues in the wild. *IEEE Transactions on Pattern Analysis and Machine Intelligence*, 2023.
- [23] Anat Levin and Yair Weiss. User assisted separation of reflections from a single image using a sparsity prior. *IEEE Transactions on Pattern Analysis and Machine Intelligence*, 29(9):1647–1654, 2007.
- [24] Yu Li and Michael S Brown. Single image layer separation using relative smoothness. In *Proceedings of the IEEE conference on computer vision and pattern recognition*, pages 2752–2759, 2014.
- [25] Yiyi Liao, Jun Xie, and Andreas Geiger. Kitti-360: A novel dataset and benchmarks for urban scene understanding in 2d and 3d. *IEEE Transactions on Pattern Analysis and Machine Intelligence*, 45(3):3292–3310, 2022.
- [26] Philipp Lindenberger, Paul-Edouard Sarlin, Viktor Larsson, and Marc Pollefeys. Pixel-Perfect Structure-from-Motion with Featuremetric Refinement. In *ICCV*, 2021.
- [27] Yu-Lun Liu, Wei-Sheng Lai, Ming-Hsuan Yang, Yung-Yu Chuang, and Jia-Bin Huang. Learning to see through obstructions. In *Proceedings of the IEEE/CVF Conference on Computer Vision and Pattern Recognition*, pages 14215–14224, 2020.
- [28] Youwei Lyu, Zhaopeng Cui, Si Li, Marc Pollefeys, and Boxin Shi. Reflection separation using a pair of unpolarized and polarized images. *Advances in neural information processing systems*, 32, 2019.
- [29] Ben Mildenhall, Pratul P Srinivasan, Matthew Tancik, Jonathan T Barron, Ravi Ramamoorthi, and Ren Ng. Nerf: Representing scenes as neural radiance fields for view synthesis. *Communications of the ACM*, 65(1):99–106, 2021.
- [30] Thomas Müller, Alex Evans, Christoph Schied, and Alexander Keller. Instant neural graphics primitives with a multiresolution hash encoding. *ACM transactions on graphics (TOG)*, 41(4):1–15, 2022.
- [31] Seonghyeon Nam, Marcus A Brubaker, and Michael S Brown. Neural image representations for multi-image fusion and layer separation. In *European conference on computer vision*, pages 216–232. Springer, 2022.
- [32] Jiaxiong Qiu, Peng-Tao Jiang, Yifan Zhu, Ze-Xin Yin, Ming-Ming Cheng, and Bo Ren. Looking through the glass: Neural surface reconstruction against high specular reflections. In *Proceedings of the IEEE/CVF Conference on Computer Vision and Pattern Recognition*, pages 20823–20833, 2023.
- [33] Grand View Research. Dashboard camera market size, share & trends analysis report by technology (basic, advanced, smart), by product, by video quality, by application, by distribution channel, by region, and segment forecasts, 2024 - 2030, 2023. Accessed: 2024-05-16.

- [34] Paul-Edouard Sarlin, Cesar Cadena, Roland Siegwart, and Marcin Dymczyk. From coarse to fine: Robust hierarchical localization at large scale. In *CVPR*, 2019.
- [35] Yoav Y Schechner, Joseph Shamir, and Nahum Kiryati. Polarization-based decorrelation of transparent layers: The inclination angle of an invisible surface. In *Proceedings of the seventh IEEE international conference on computer vision*, volume 2, pages 814–819. IEEE, 1999.
- [36] Johannes L Schönberger, Enliang Zheng, Jan-Michael Frahm, and Marc Pollefeys. Pixelwise view selection for unstructured multi-view stereo. In *Computer Vision—ECCV 2016: 14th European Conference, Amsterdam, The Netherlands, October 11–14, 2016, Proceedings, Part III 14*, pages 501–518. Springer, 2016.
- [37] YiChang Shih, Dilip Krishnan, Fredo Durand, and William T Freeman. Reflection removal using ghosting cues. In *Proceedings of the IEEE conference on computer vision and pattern recognition*, pages 3193–3201, 2015.
- [38] Christian Simon and In Kyu Park. Reflection removal for in-vehicle black box videos. In *Proceedings of the IEEE Conference on Computer Vision and Pattern Recognition*, pages 4231–4239, 2015.
- [39] Chao Sun, Shuaicheng Liu, Taotao Yang, Bing Zeng, Zhengning Wang, and Guanghui Liu. Automatic reflection removal using gradient intensity and motion cues. *Proceedings of the 24th ACM international conference on Multimedia*, 2016.
- [40] Deqing Sun, Xiaodong Yang, Ming-Yu Liu, and Jan Kautz. Pwc-net: Cnns for optical flow using pyramid, warping, and cost volume. *2018 IEEE/CVF Conference on Computer Vision and Pattern Recognition*, pages 8934–8943, 2017.
- [41] Pei Sun, Henrik Kretzschmar, Xerxes Dotiwalla, Aurelien Chouard, Vijaysai Patnaik, Paul Tsui, James Guo, Yin Zhou, Yuning Chai, Benjamin Caine, et al. Scalability in perception for autonomous driving: Waymo open dataset. In *Proceedings of the IEEE/CVF conference on computer vision and pattern recognition*, pages 2446–2454, 2020.
- [42] Richard Szeliski, Shai Avidan, and Padmanabhan Anandan. Layer extraction from multiple images containing reflections and transparency. In *Proceedings IEEE Conference on Computer Vision and Pattern Recognition. CVPR 2000 (Cat. No. PR00662)*, volume 1, pages 246–253. IEEE, 2000.
- [43] Matthew Tancik, Vincent Casser, Xinchun Yan, Sabeek Pradhan, Ben Mildenhall, Pratul P Srinivasan, Jonathan T Barron, and Henrik Kretzschmar. Block-nerf: Scalable large scene neural view synthesis. In *Proceedings of the IEEE/CVF Conference on Computer Vision and Pattern Recognition*, pages 8248–8258, 2022.
- [44] Haithem Turki, Deva Ramanan, and Mahadev Satyanarayanan. Mega-nerf: Scalable construction of large-scale nerfs for virtual fly-throughs. In *Proceedings of the IEEE/CVF Conference on Computer Vision and Pattern Recognition*, pages 12922–12931, 2022.
- [45] Haithem Turki, Jason Y Zhang, Francesco Ferroni, and Deva Ramanan. Suds: Scalable urban dynamic scenes. In *Proceedings of the IEEE/CVF Conference on Computer Vision and Pattern Recognition*, pages 12375–12385, 2023.
- [46] Renjie Wan, Boxin Shi, Haoliang Li, Yuchen Hong, Ling-Yu Duan, and Alex C Kot. Benchmarking single-image reflection removal algorithms. *IEEE Transactions on Pattern Analysis and Machine Intelligence*, 45(2):1424–1441, 2022.
- [47] Fangjinhua Wang, Silvano Galliani, Christoph Vogel, Pablo Speciale, and Marc Pollefeys. Patchmatchnet: Learned multi-view patchmatch stereo. In *Proceedings of the IEEE/CVF conference on computer vision and pattern recognition*, pages 14194–14203, 2021.
- [48] Zhou Wang, Alan C Bovik, Hamid R Sheikh, and Eero P Simoncelli. Image quality assessment: from error visibility to structural similarity. *IEEE transactions on image processing*, 13(4):600–612, 2004.

- [49] Kaixuan Wei, Jiaolong Yang, Ying Fu, David Wipf, and Hua Huang. Single image reflection removal exploiting misaligned training data and network enhancements. In *Proceedings of the IEEE/CVF Conference on Computer Vision and Pattern Recognition*, pages 8178–8187, 2019.
- [50] Zirui Wu, Tianyu Liu, Liyi Luo, Zhide Zhong, Jianteng Chen, Hongmin Xiao, Chao Hou, Haozhe Lou, Yuantao Chen, Runyi Yang, et al. Mars: An instance-aware, modular and realistic simulator for autonomous driving. In *CAAI International Conference on Artificial Intelligence*, pages 3–15. Springer, 2023.
- [51] Ziyang Xie, Junge Zhang, Wenye Li, Feihu Zhang, and Li Zhang. S-nerf: Neural radiance fields for street views. *arXiv preprint arXiv:2303.00749*, 2023.
- [52] Jiawei Yang, Boris Ivanovic, Or Litany, Xinshuo Weng, Seung Wook Kim, Boyi Li, Tong Che, Danfei Xu, Sanja Fidler, Marco Pavone, et al. Emernerf: Emergent spatial-temporal scene decomposition via self-supervision. *arXiv preprint arXiv:2311.02077*, 2023.
- [53] Jie Yang, Dong Gong, Lingqiao Liu, and Qinfeng Shi. Seeing deeply and bidirectionally: A deep learning approach for single image reflection removal. In *Proceedings of the european conference on computer vision (ECCV)*, pages 654–669, 2018.
- [54] Yang Yang, Wenye Ma, Yin Zheng, Jian-Feng Cai, and Weiyu Xu. Fast single image reflection suppression via convex optimization. In *Proceedings of the IEEE/CVF conference on computer vision and pattern recognition*, pages 8141–8149, 2019.
- [55] Ze Yang, Yun Chen, Jingkan Wang, Sivabalan Manivasagam, Wei-Chiu Ma, Anqi Joyce Yang, and Raquel Urtasun. Unisim: A neural closed-loop sensor simulator. In *Proceedings of the IEEE/CVF Conference on Computer Vision and Pattern Recognition*, pages 1389–1399, 2023.
- [56] Ziyi Yang, Xinyu Gao, Wen Zhou, Shaohui Jiao, Yuqing Zhang, and Xiaogang Jin. Deformable 3d gaussians for high-fidelity monocular dynamic scene reconstruction. *arXiv preprint arXiv:2309.13101*, 2023.
- [57] Fisher Yu, Haofeng Chen, Xin Wang, Wenqi Xian, Yingying Chen, Fangchen Liu, Vashisht Madhavan, and Trevor Darrell. Bdd100k: A diverse driving dataset for heterogeneous multitask learning. In *Proceedings of the IEEE/CVF conference on computer vision and pattern recognition*, pages 2636–2645, 2020.
- [58] Oliver Zendel, Katrin Honauer, Markus Murschitz, Daniel Steininger, and Gustavo Fernandez Dominguez. Wilddash-creating hazard-aware benchmarks. In *Proceedings of the European Conference on Computer Vision (ECCV)*, pages 402–416, 2018.
- [59] Kai Zhang, Gernot Riegler, Noah Snaveley, and Vladlen Koltun. Nerf++: Analyzing and improving neural radiance fields. *arXiv preprint arXiv:2010.07492*, 2020.
- [60] Richard Zhang, Phillip Isola, Alexei A Efros, Eli Shechtman, and Oliver Wang. The unreasonable effectiveness of deep features as a perceptual metric. In *Proceedings of the IEEE conference on computer vision and pattern recognition*, pages 586–595, 2018.
- [61] Xiaoshuai Zhang, Abhijit Kundu, Thomas Funkhouser, Leonidas Guibas, Hao Su, and Kyle Genova. Nerflets: Local radiance fields for efficient structure-aware 3d scene representation from 2d supervision. In *Proceedings of the IEEE/CVF Conference on Computer Vision and Pattern Recognition*, pages 8274–8284, 2023.
- [62] Xuaner Zhang, Ren Ng, and Qifeng Chen. Single image reflection separation with perceptual losses. In *Proceedings of the IEEE conference on computer vision and pattern recognition*, pages 4786–4794, 2018.
- [63] MI Zhenxing and Dan Xu. Switch-nerf: Learning scene decomposition with mixture of experts for large-scale neural radiance fields. In *The Eleventh International Conference on Learning Representations*, 2022.
- [64] Hongyu Zhou, Jiahao Shao, Lu Xu, Dongfeng Bai, Weichao Qiu, Bingbing Liu, Yue Wang, Andreas Geiger, and Yiyi Liao. Hugs: Holistic urban 3d scene understanding via gaussian splatting. *arXiv preprint arXiv:2403.12722*, 2024.

- [65] Xiaoyu Zhou, Zhiwei Lin, Xiaojun Shan, Yongtao Wang, Deqing Sun, and Ming-Hsuan Yang. Drivinggaussian: Composite gaussian splatting for surrounding dynamic autonomous driving scenes. *arXiv preprint arXiv:2312.07920*, 2023.
- [66] Chengxuan Zhu, Renjie Wan, and Boxin Shi. Neural transmitted radiance fields. *Advances in Neural Information Processing Systems*, 35:38994–39006, 2022.
- [67] Chengxuan Zhu, Renjie Wan, Yunkai Tang, and Boxin Shi. Occlusion-free scene recovery via neural radiance fields. In *Proceedings of the IEEE/CVF Conference on Computer Vision and Pattern Recognition*, pages 20722–20731, 2023.
- [68] Matthias Zwicker, Hanspeter Pfister, Jeroen Van Baar, and Markus Gross. Ewa splatting. *IEEE Transactions on Visualization and Computer Graphics*, 8(3):223–238, 2002.

A Appendix / supplemental material

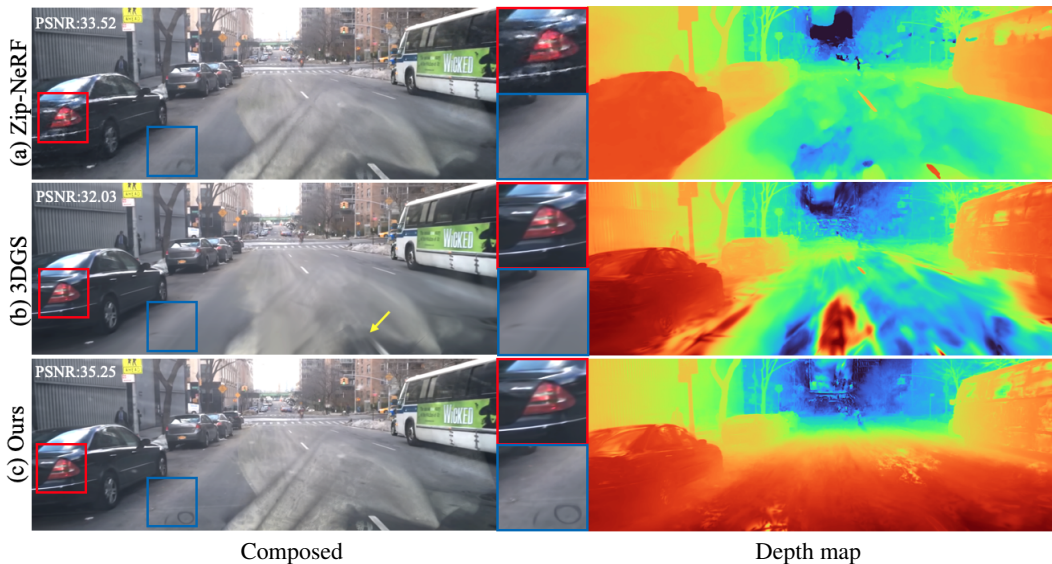


Figure 9: Comparisons with 3DGS and Zip-NeRF [4] on novel view synthesis show that obstructions violate multi-view consistency, leading to erroneous geometry in 3DGS and Zip-NeRF, as evident in the depth maps. This results in blurry renderings and artifacts. In contrast, our method effectively addresses the ambiguity introduced by obstructions and learns physically reasonable geometry, achieving renderings with fine details.

Table 3: Ablation on threshold τ used in Eq. 7. Our results are not sensitive to the choice of τ .

τ	PSNR \uparrow	SSIM \uparrow	LPIPS \downarrow
0.3	26.27	0.814	0.210
0.5	26.30	0.814	0.210
0.7	26.28	0.814	0.210

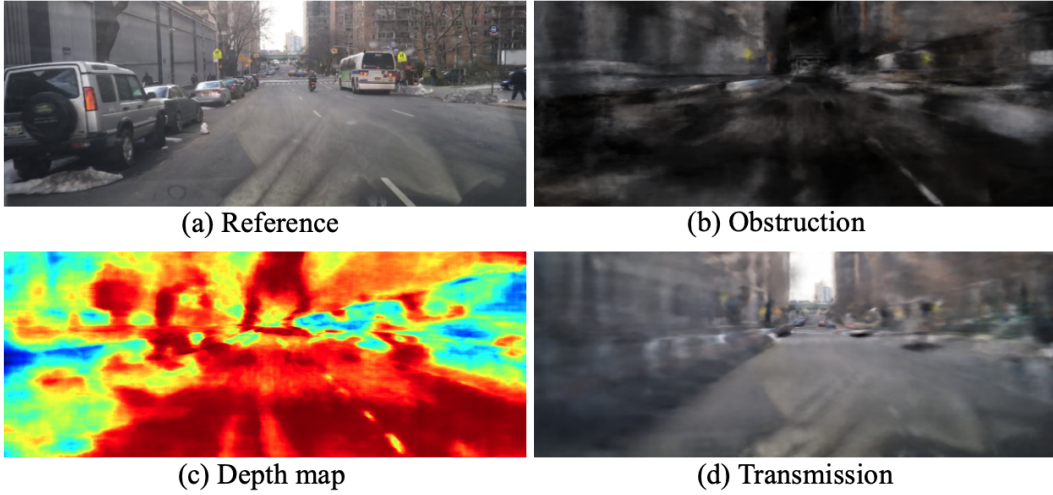


Figure 10: We evaluate NeRFren [16] on our curated dataset. The suboptimal results of NeRFren are caused by two factors. First, its obstruction modeling cannot address the ambiguity between obstructions and transmission, leading to a failure in image decomposition. Second, its backbone, NeRF, cannot handle large-scale driving scenes, resulting in blurry outputs.

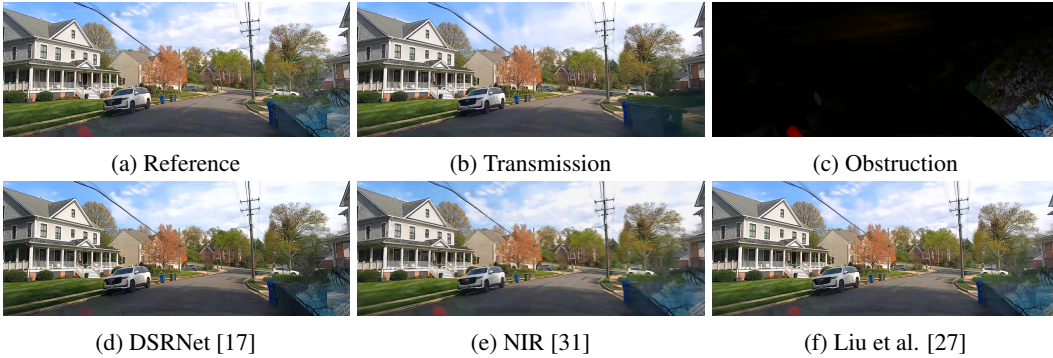


Figure 11: Comparisons with image-based reflection removal methods show that our method achieves significantly better results than previous methods [17, 31, 27] in removing reflections.

Table 4: We first use DSRNet [17] to remove reflections from the input images, and then we train and evaluate 3DGS [19] on these images. The results show that due to the insufficiency of the reflection removal, novel view synthesis performance cannot be improved in this way.

Method	BDD100K			DCVR		
	PSNR \uparrow	SSIM \uparrow	LPIPS \downarrow	PSNR \uparrow	SSIM \uparrow	LPIPS \downarrow
3DGS	28.02	0.897	0.188	23.73	0.783	0.248
3DGS + DSRNet	27.99	0.898	0.188	23.72	0.783	0.248